Cerebral ^{18}F-FDG PET/CT Metabolism as Diagnostic Signature for Central Nervous System Toxicity After Immune Checkpoint Blockade Cancer Treatment

Yifei Ma*[1], Jiling Zeng*[2,3], Fadian Ding*[1], Yiwei Xu[4], Youlong Wang[5], Guanqing Zhong[6], Nianqi Liu[7], Yanqi Wang[8,9], Yiming Li[10], Shuqin Chen[11], Xiaolong Wei[11], Pengfei Zhu[12], Guangmin Jian[12], Yu Si Niu[13], Guangzhen Fu[14], Cantong Liu[4], Guiqiang Li[8], Xiaotong Zhou[15], Ao Zhang[3,6], and Shangeng Weng[1]

[1]Department of Hepatobiliary and Pancreatic Surgery, Institute of Abdominal Surgery, Fujian Provincial Key Laboratory of Precision Medicine for Cancer, and Department of Hepatobiliary and Pancreatic Surgery, National Regional Medical Center Binhai Campus, First Affiliated Hospital of Fujian Medical University, Fuzhou, China; [2]Department of Nuclear Medicine, State Key Laboratory of Oncology in South China, Collaborative Innovation Center for Cancer Medicine, Guangzhou, China; [3]State Key Laboratory of Oncology in South China, Guangdong Key Laboratory of Nasopharyngeal Carcinoma Diagnosis and Therapy, Guangdong Provincial Clinical Research Center for Cancer, Guangzhou, China; [4]Department of Clinical Laboratory Medicine, Cancer Hospital of Shantou University Medical College, Shantou, China; [5]Department of General Surgery, Hainan Hospital of People's Liberation Army General Hospital, Sanya, China; [6]Department of Clinical Laboratory, State Key Laboratory of Oncology in South China, Collaborative Innovation Center for Cancer Medicine, Guangdong Key Laboratory of Nasopharyngeal Carcinoma Diagnosis and Therapy, Sun Yat-Sen University Cancer Center, Guangzhou, China; [7]Faculty of Psychology, Institute of Educational Science, Huazhong University of Science and Technology, Wuhan, China; [8]Department of Orthopedics and Spine Surgery, Second Affiliated Hospital of Shantou University Medical College, Shantou, China; [9]School of Public Health, Shantou University, Shantou, China; [10]Department of Neurosurgery, Beijing Tiantan Hospital Capital Medical University, Beijing, China; [11]Department of Pathology, Cancer Hospital of Shantou University Medical College, Shantou, China; [12]Department of Clinical Laboratory, First Affiliated Hospital of Zhengzhou University, Zhengzhou, China; [13]Acute Communicable Disease Epidemiology Division, Dallas County Health and Human Services, Dallas, Texas; [14]Key Clinical Laboratory of Henan Province, First Affiliated Hospital of Zhengzhou University, Zhengzhou, China; and [15]Department of Bone and Soft Tissue Oncology, Cancer Hospital of Shantou University Medical College, Shantou, China

Our aim was to investigate probable biomarkers specific to immune-related central nervous system toxicity (CNST) in cancer patients treated with immune checkpoint inhibitors (ICI) by analysis of ^{18}F-FDG PET/CT images. **Methods:** Cancer patients receiving ICI treatment were enrolled in a multicenter observational study that analyzed regional metabolic changes before and during CNST onset from January 2020 to February 2022. In 1:1 propensity score–matched pairs, the regional SUV_{mean} of each bilateral brain lobe of CNST patients (CNST+) was compared with that of patients who had central nervous system infections (CNSIs) and patients without CNST or CNSI (CNST−). In a validation cohort, patients were recruited from February 2022 to July 2023 and followed up for 24 wk after the start of ICI. Early changes in regional SUV_{mean} at 5–6 wk after therapy initiation were evaluated for ability to predict later CNST onset. **Results:** Of 6,395 ICI-treated patients, 2,387 underwent prognostic ^{18}F-FDG PET/CT and 125 of the scanned patients had CNST (median time from ICI treatment to onset, 9 wk; quartile range, 2–23 wk). Regional ^{18}F-FDG PET/CT SUV_{mean} changes were higher in CNST+ than in CNST− patients (117 patient pairs) but were lower than in CNSI patients (50 pairs). Differentiating analysis reached an area under the curve (AUC) of 0.83 (95% CI, 0.78–0.88) for CNST+ versus CNST− and of 0.80 (95% CI, 0.72–0.89) for CNST+ versus CNSI. Changes in SUV_{mean} were also higher before CNST onset than for CNST− (60 pairs; AUC, 0.74; 95% CI, 0.66–0.83). In a validation cohort of 2,878 patients, preonset changes in SUV_{mean} reached an AUC of 0.86 (95% CI, 0.79–0.94) in predicting later CNST incidence. **Conclusion:** Brain regional hypermetabolism could be detected during and before CNST clinical onset. CNST may be a distinct pathologic entity versus brain infections defined by ^{18}F-FDG PET/CT brain scans. Regional SUV differences may be translated into early diagnostic tools based on moderate differentiating accuracy in our study.

Key Words: ^{18}F-FDG PET/CT brain imaging; immunotherapy; immune-related CNS toxicity; regional metabolism; differential diagnosis

Immune checkpoint inhibitors (ICIs) have revolutionized the therapeutic landscape and significantly prolonged survival during the past decade, making ICI one of the primary therapies in nearly all types of cancer (1). ICIs inflict immune-related adverse events due to systemic T-cell activation, which can happen in any organ and have been reported to have an incidence of 10%–90% for any grade (2–4). However, immune-related adverse events in the central nervous system, or central nervous system toxicity (CNST), are less prevalent than in other organs, with an incidence of 1%–8% reported previously and fewer than 1% of cases being fatal (5,6). CNST has varieties of pathology types, including but not limited to immune-related meningitis, encephalitis, demyelinating encephalopathy, and central nervous system vasculitis (7). Although the exact pathoetiology is not thoroughly known, CNST

is currently suggested to be induced by local inflammation from deranged immune attack (8).

CNST presents mostly with unspecific symptoms, including headaches (>50%), confusion, partial seizures, limb pain, and the meningeal irritation sign (9). Given the higher incidence of central nervous system infection (CNSI) in cancer patients and significant overlapping symptoms, CNST is usually diagnosed when other causes are excluded, including infection, brain hemorrhage, stroke, metabolic encephalopathy, and brain metastasis (10). Methods applied in clinical diagnosis involve traditional imaging protocols, cerebral spinal fluid analysis, and neurologic work-ups (10). According to the Consensus Statement of Neurologic Adverse Events, most suspected cases are given a possible diagnosis for further trial therapies because of the difficulty of making a definite diagnosis (8). Because of the unpredictable incidence of this severe complication during ICI treatment, which many patients may receive for years, the development of biomarkers for early diagnosis is crucial (11). However, efficient methods and predictable biomarkers for differential diagnosis are presently lacking, hindering subsequent management options.

^{18}F-FDG PET/CT is a noninvasive imaging tool applied in diagnostic and prognostic protocols for cancer patients. Besides its utility in cancer management, the high sensitivity of ^{18}F-FDG PET/CT imaging has long been well established for identifying inflammatory processes involving higher local metabolism (12). Anecdotal case reports of ^{18}F-FDG PET/CT imaging analysis in evaluations of immune-related adverse events are being reported, but the characteristics of CNST have not been extensively reviewed (13). A pilot retrospective study of 58 melanoma patients identified metabolic biomarkers to delineate patients with or without immune-related adverse events in the lung, colon, and thyroid gland (14). Furthermore, ^{18}F-FDG PET/CT imaging is capable of sensitively detecting local autoimmune attacks in cerebral regions and has been established as an alternative tool to diagnose autoimmune or paraneoplastic encephalitis (15,16). More direct evidence was found in a recent ^{18}F-FDG PET/CT study of anti-LG1 protein autoimmune encephalitis, which is pathologically similar to CNST; biomarkers were identified that can signify disease course (17). Thus, we hypothesize that brain metabolism may be characteristic in patients with CNST (18,19).

Because of the low incidence of CNST, pivotal research on diagnostic biomarker identification for CNST has been statistically difficult to perform in underpowered sample sizes (20). Nevertheless, as ICIs are becoming more available in real-world settings, pilot multicenter analysis is encouraged to identify markers in the growing number of CNST cases. In the current study, we retrospectively reviewed cerebral metabolism in ICI-treated cancer patients, with the aim of obtaining preliminary evidence of diagnostic biomarkers for subclinical or syndromal CNST.

MATERIALS AND METHODS

Participants and Eligibility Criteria

We performed a multicenter, retrospective, case-control study to analyze early CNST-related metabolic changes in cerebral ^{18}F-FDG

PET/CT images of ICI-treated cancer patients, who were divided into a discovery cohort and a validation cohort. In the discovery cohort, cancer patients receiving ICI treatment were enrolled from January 2020 to February 2022, and in the validation cohort, patients were enrolled from February 2022 to July 2023. Demographic and clinical variables were recorded from chart review. The research setting was the nuclear medicine departments of 4 academic hospitals in China (supplemental materials, available at http://jnm.snmjournals.org) (21–28). The retrospective protocol of the study was approved by the institutional review board of the Affiliated Cancer Hospital of Shantou University Medical College. All procedure was performed according to the Helsinki Declaration. The participants had given written informed consent to use of clinical information for medical research. Reporting adhered to the Strengthening the Reporting of Observational Studies in Epidemiology checklist for cohort studies.

Chart review divided ICI-treated cancer patients into 3 groups: patients with CNST (CNST+ group), with CNSI (CNSI group), and without CNST or CNSI (CNST− group, defined as no CNST or CNSI for ≥5 mo after ICI treatment, as most patients developed CNST before 20 wk as previously described) (29). The diagnostic protocols for CNST were according to the Consensus Statement of Neurologic Adverse Events (the supplemental materials provide detailed criteria) (8). All symptoms related to diagnosis and excluding CNST followed Common Terminology Criteria for Adverse Events (version 5.0). The date of CNST diagnosis was identified by review of outpatient and inpatient charts.

Research Goals and Statistics

The research goals are illustrated in Figure 1A. We did 2 independent comparison analyses (between the CNST+ and CNST− groups and between the CNST+ and CNSI groups) to investigate the specificity of cerebral regional SUV$_{mean}$ in CNST+ patients. First, regional SUV$_{mean}$ changes was calculated and compared between the CNST+ group (calculated as the SUV$_{mean}$ difference between baseline and CNST onset) and the CNST− group (serving as a negative control comparison). Second, the SUV$_{mean}$ of subtype CNST was compared with the SUV$_{mean}$ of subtype CNSI (serving as a positive control comparison). For each step, a principal-component analysis and a neural network computation model were adopted to evaluate the differentiating ability of regional SUV$_{mean}$ in ^{18}F-FDG PET/CT scans.
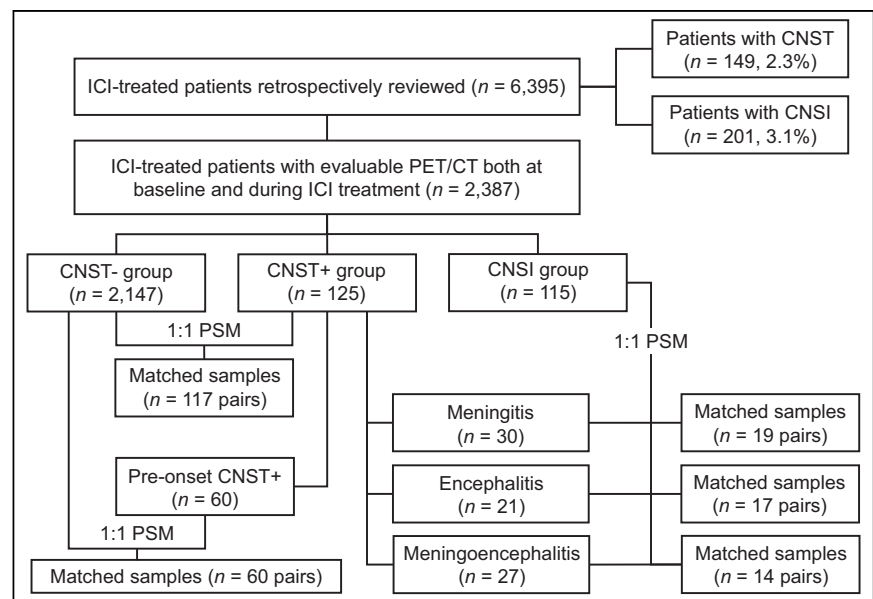

FIGURE 1. Research flowchart.

TABLE 1
Baseline Variables Before and After Propensity Score Matching for CNST+ and CNST− Subtypes

Variable	Before matching (n = 2,272)			After matching (n = 117 pairs)			
	CNST+ (n = 125)	CNST− (n = 2,147)	P*	CNST+	CNST−	SMD	P[†]
Age	59.71 (10.21)	57.82 (12.28)	0.05	59.25 (10.07)	59.84 (11.28)	0.06	0.76
Body mass index	22.90 (3.20)	23.23 (3.00)	0.24	22.80 (3.20)	23.18 (3.04)	0.12	0.23
Male sex	82 (65.6)	1169 (54.4)	0.02	75 (64.1)	77 (65.8)	0.04	0.88
Positive smoking history	38 (30.4)	510 (23.8)	0.09	38 (32.5)	33 (28.2)	0.09	0.54
Abnormal CRP	10 (8.0)	214 (10.0)	0.47	10 (8.5)	13 (11.1)	0.09	0.66
Concurrent target therapy	29 (23.2)	531 (24.7)	0.70	28 (23.9)	21 (17.9)	0.14	0.35
Concurrent chemotherapy	63 (50.4)	875 (40.8)	0.03	56 (47.9)	56 (47.9)	<0.01	1.00
Radiotherapy history	5 (4.0)	153 (7.1)	0.18	5 (4.3)	5 (4.3)	<0.01	1.00
Primary surgery	108 (86.4)	1609 (74.9)	<0.01	100 (85.5)	95 (81.2)	0.12	0.44
Stage of I and II	53 (42.4)	894 (41.6)	0.82	49 (41.9)	50 (42.8)	0.03	0.59
Comorbid neurologic disease	8 (6.4)	127 (5.9)	0.82	8 (6.8)	5 (4.3)	0.10	0.58
Comorbid CHF	7 (5.6)	123 (5.7)	0.95	4 (3.4)	4 (3.4)	<0.01	1.00
ECOG score	2 (1.06)	2.19 (1.09)	0.06	2.01 (1.03)	2.04 (1.20)	0.03	0.98
Positive mental problem	31 (24.8)	609 (28.4)	0.39	30 (25.6)	33 (28.2)	0.06	0.67
Treatment							
Atezolizumab	13 (7.0)	264 (12.3)	<0.01	12 (10.3)	15 (12.8)	0.02	0.83
Camrelizumab	7 (5.6)	274 (12.8)		7 (6.0)	7 (6.0)	<0.01	
Durvalumab	8 (6.4)	113 (5.3)		7 (6.0)	5 (4.3)	0.07	
Nivolumab	24 (19.2)	540 (25.2)		24 (20.5)	31 (26.5)	0.15	
Pembrolizumab	22 (17.6)	235 (10.9)		20 (17.1)	22 (18.8)	0.04	
Sintilimab	35 (28.0)	610 (28.4)		33 (28.2)	26 (22.2)	0.13	
Toripalimab	16 (12.8)	111 (5.2)		14 (12.0)	11 (9.4)	0.08	
Cancer type							
Nasopharyngeal carcinoma	8 (6.4)	175 (8.2)	0.06	8 (6.8)	6 (5.1)	0.07	0.96
Non–small cell lung cancer	41 (31.8)	555 (25.9)		39 (33.3)	42 (35.9)	0.05	
Colorectal carcinoma	19 (15.2)	187 (8.7)		15 (12.8)	16 (13.7)	0.02	
Gastric cancers	3 (2.4)	78 (3.6)		0 (0.0)	3 (2.6)	0.17	
Hepatocellular carcinoma	5 (4.0)	92 (4.3)		5 (4.3)	7 (6.0)	0.09	
Oral carcinoma	2 (1.6)	96 (4.5)		2 (1.7)	2 (1.7)	<0.01	
Biliary and pancreatic cancers	3 (2.4)	101 (4.7)		3 (2.6)	2 (1.7)	0.06	
Sarcoma	2 (1.6)	86 (4.0)		5 (4.3)	2 (1.7)	0.07	
Renal cell carcinoma	6 (4.8)	128 (6.0)		6 (5.1)	7 (6.0)	0.03	
Urogenital cancers	3 (2.4)	103 (4.8)		3 (2.6)	3 (2.6)	<0.01	
Mesothelioma	4 (3.2)	136 (6.3)		4 (3.4)	4 (3.4)	0.04	
Lymphoma	11 (8.8)	173 (8.1)		10 (8.5)	9 (7.7)	<0.01	
Other cancer types	8 (6.4)	147 (6.8)		8 (6.8)	6 (5.1)	0.2	
Unknown cancer types	10 (8.0)	90 (4.2)		9 (7.7)	8 (6.8)	0.03	
Whole-brain SUV$_{mean}$	4.40 (1.35)	5.75 (1.39)	<0.01	4.57 (1.21)	4.48 (1.26)	0.07	0.27

*Independent t test (continuous) or χ^2 test (categoric).

[†]Wilcoxon signed-rank test (continuous), McNemar nonparametric test (binary), and χ^2 test (multiple categories).

SMD = standardized mean difference to show imbalance levels of variables after matching (variable with SMD > 0.25 is considered poorly matched); CRP = C-reactive protein; CHF = congestive heart failure; ECOG = Eastern Cooperative Oncology Group.

Data are number followed by percentage in parentheses, except for whole-brain SUV$_{mean}$, for which SD is given in parentheses.

Third, for the CNST+ subgroup analysis, we queried whether there were early changes in brain metabolism before CNST symptoms started. To minimize the false-positive rate, subgroup analysis in the CNST+ group included only patients who underwent ^{18}F-FDG PET/CT at least 4 wk before CNST onset (i.e., preonset). Changes in SUV_{mean} from the baseline ^{18}F-FDG PET/CT images to the preonset images in CNST+ patients were calculated and compared with changes in SUV_{mean} in the CNST− group. If multiple images were present, only the earliest image was analyzed. A neural network computation model was adopted to evaluate the differentiating ability of regional SUV_{mean} in ^{18}F-FDG PET/CT scans. Last, in an independent validation cohort, preonset regional SUV_{mean} changes at 5–6 wk after ICI initiation were evaluated in a real-world setting to determine whether they may predict the later incidence of CNST, and a nomogram was built to quantify the disease-free (CNST-free) survival probability. Statistical comparison, propensity score matching, and modeling details of the neural network computation are shown in the supplemental materials (22,23,27).

RESULTS

Demographics

The study on the discovery cohort included 6,395 patients who had ever received ICI therapy and 2,387 patients who had evaluable ^{18}F-FDG PET/CT scans both at baseline and during ICI treatment. One hundred forty-nine patients had CNST (incidence, 2.3%), and 125 patients had evaluable ^{18}F-FDG PET/CT scans (Fig. 1A). Briefly, there were 125 CNST+ patients in the imaging study (69.3% male), with a mean age of 59.71 y (SD, 10.21 y), spanning nearly all known cancer types and ICI types. Baseline information was substantially different from that in the CNST− group, and 1:1 propensity score matching (PSM) was performed for balancing. Of the 125 CNST+ patients, 117 were matched with 117 CNST− patients. Baseline information before and after propensity score matching is shown in Table 1. Additional details on CNST characteristics are shown in Supplemental Table 1. Blood glucose levels in comparable groups are shown in Supplemental Figure 1, and representative images are shown in Supplemental Figure 2.

Regional Uptake Values of CNST+ Compared with CNST− Patients

We first investigated metabolic changes in patients experiencing CNST in each brain region. By the Wilcoxon signed-rank test, there was a significant increase ($P < 0.01$) in SUV_{mean} from baseline to CNST onset in all regions except the brain stem, occipital lobe, and cerebellum (Supplemental Fig. 3A, power of statistical tests reached >0.90 assuming a 2-sided α of 0.05). The median value of whole-brain SUV_{mean} in the CNST− group did not significantly differ from baseline, but this statistical test was underpowered ($P = 0.06$; power, 0.31). We then compared changes in both groups in PSM pairs. Compared with CNST− patients, there were significantly more increases in SUV_{mean} in each region of CNST+ patients except in the brain stem, occipital lobe, and cerebellum (Fig. 2A). Principal-component analysis indicated a

relatively poor differentiating ability between the CNST+ and CNST− groups ($R = 0.14$, Supplemental Fig. 4A). However, the calculated differentiating ability from the neural network computation-based model showed an area under the curve (AUC) of 0.83 (95% CI, 0.78–0.88; Supplemental Fig. 4B). Principal-component analysis of CNST subtypes indicated an R of 0.64 (Fig. 2B).

Regional Uptake Values of CNST+ Subtypes Compared with CNSI Subtypes

Clinical symptoms and imaging studies of CNST may mimic CNSI, and thus we tested the specificity of CNST regional uptake values by comparing CNST+ with PSM samples of CNSI subtypes: immune-related versus infectious meningitis, meningoencephalitis, and encephalitis. In total, 201 patients who had a diagnosis of CNSI were reviewed, 115 of whom had available ^{18}F-FDG PET/CT images during CNSI onset. We adopted optimal matching for 3 subtypes between CNST+ and CNSI. Nearest-neighbor matching was adopted for other baseline variables. Finally, 50 pairs were matched from 3 subtypes of CNST+ and CNSI patients, including 19 pairs of meningitis, 17 pairs of meningoencephalitis, and 14 pairs of encephalitis, with baseline demographic details before and after PSM shown in Table 2. The regional SUV_{mean} of the immune-related meningitis subtype was significantly lower than that of infectious meningitis in all regions of interest (Fig. 3A). In the meningoencephalitis subtype, regional values were also lower in CNST+ patients in nearly all regions, except for the brain stem and cerebellum (Fig. 3B). In the encephalitis subtype, a significantly lower SUV_{mean} was seen in the whole brain and in the limbic area in CNST+ patients, although a higher SUV_{mean} was seen in the parietal region of CNST+ patients (Fig. 3C). Principal-component analysis indicated a moderate to high ability to differentiate the 3 subtypes between CNST+ and CNSI (Figs. 3D–3F). Differential diagnostic tests of the neural network computation-based radiomic model indicated relatively good accuracy (AUC, 0.80; 95% CI, 0.72–0.89; Supplemental Fig. 5A).
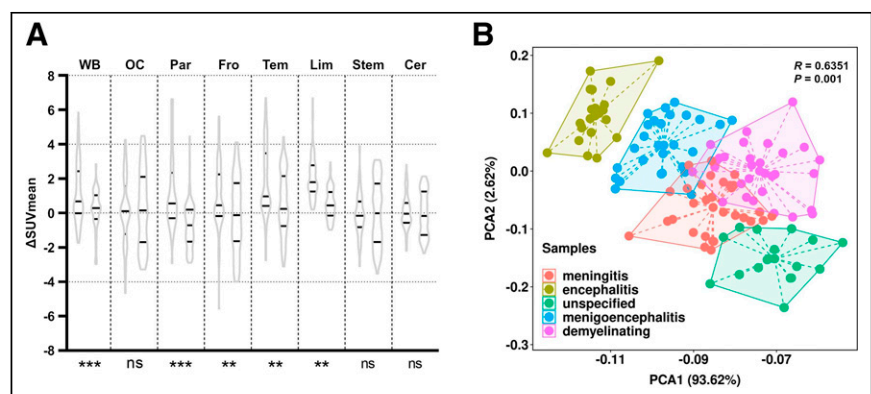

FIGURE 2. Comparison analysis of regional uptake value changes with negative control. (A) Negative control comparison: changes in SUV_{mean} from baseline to disease onset in CNST+ patients (left side of plot for each region) and changes in SUV_{mean} from baseline to >5 mo after treatment in negative control (right side of plot for each region), matched by propensity scores. Black lines indicate median and range (first to third quartiles). Nonparametric Wilcoxon signed-rank test was performed to compare distribution. Significant difference in changes in SUV_{mean} was seen between 2 groups in whole-brain area and in parietal, frontal, temporal, and limbic regions. (B) Principal-component analysis of ^{18}F-FDG PET/CT radiomic uptake values to differentiate CNST subtypes in CNST+ patients ($R = 0.64$). Cer = cerebellum; fro = frontal lobe; lim = limbic area; ns = nonsignificant; OC = occipital lobe; par = parietal lobe; PCA = principal-component analysis; stem = brain stem; tem = temporal lobe; WB = whole brain. *$P < 0.05$. **$P < 0.01$. ***$P < 0.001$.

TABLE 2
Baseline Variables Before and After Propensity Score Matching for CNST+ and CNSI Subtypes

Variable	Before matching (n = 193)			After matching (n = 50 pairs)			
	CNST+ (n = 78)	CNSI (n = 115)	P*	CNST+	CNSI	SMD	P†
Age	59.15 (10.85)	53.63 (14.25)	<0.01	56.66 (11.37)	59.12 (9.43)	0.23	0.50
Body mass index	23.23 (3.33)	22.97 (1.12)	0.43	22.76 (3.27)	22.92 (1.14)	0.05	0.81
Male sex	50 (64.1)	68 (59.1)	0.49	31 (62.0)	31 (62.0)	<0.01	1.00
Positive smoking history	22 (28.2)	28 (24.3)	0.55	14 (28.0)	13 (26.0)	0.04	1.00
Meningitis	30 (38.5)	38 (33.0)	0.70	19 (38.0)	19 (38.0)	<0.01	1.00
Encephalitis	21 (26.9)	36 (31.3)		17 (34.0)	17 (34.0)	<0.01	
Meningoencephalitis	27 (34.6)	41 (35.7)		14 (28.0)	14 (28.0)	<0.01	
Concurrent target therapy	22 (28.2)	32 (27.8)	0.95	11 (22.0)	10 (20.0)	0.04	1.00
Concurrent chemotherapy	39 (50.0)	57 (49.6)	0.95	27 (54.0)	30 (60.0)	0.12	0.68
Radiotherapy history	3 (3.8)	6 (5.2)	0.66	2 (4.0)	3 (6.0)	0.10	1.00
Primary surgery	66 (84.6)	91 (79.1)	0.34	44 (88.0)	43 (86.0)	0.06	1.00
Stage of I and II	28 (35.9)	47 (50.9)	0.91	18 (36.0)	20 (40.0)	0.11	0.80
Comorbid neurologic disease	4 (5.1)	9 (7.8)	0.46	3 (6.0)	3 (6.0)	<0.01	1.00
Comorbid CHF	3 (3.8)	7 (6.1)	0.49	1 (2.0)	1 (2.0)	<0.01	1.00
ECOG score	1.94 (1.15)	2.28 (1.20)	0.05	2.08 (1.10)	2.06 (1.19)	0.02	0.95
Positive mental problem	23 (29.5)	33 (28.7)	0.91	15 (30.0)	13 (26.0)	0.09	0.83
Treatment							
Atezolizumab	9 (11.5)	8 (7.0)	0.37	6 (12.0)	4 (8.0)	0.12	0.92
Camrelizumab	5 (6.4)	7 (6.1)		3 (6.0)	2 (4.0)	0.08	
Durvalumab	7 (9.0)	10 (8.7)		6 (12.0)	5 (10.0)	0.07	
Nivolumab	15 (19.2)	17 (14.8)		12 (24.0)	9 (18.0)	0.15	
Pembrolizumab	12 (15.4)	15 (13.0)		6 (12.0)	8 (16.0)	−0.11	
Sintilimab	21 (26.9)	34 (29.6)		11 (22.0)	14 (28.0)	−0.13	
Tislelizumab	0 (0.0)	8 (7.0)		0 (0.0)	0 (0.0)	NA	
Toripalimab	9 (11.5)	16 (13.9)		6 (12.0)	8 (16.0)	−0.12	
Cancer type							
Nasopharyngeal carcinoma	2 (2.6)	15 (13.0)	0.07	2 (4.0)	4 (8.0)	0.18	0.90
Non–small cell lung cancer	25 (32.1)	23 (20.0)		15 (30.0)	13 (26.0)	0.09	
Colorectal carcinoma	14 (17.9)	19 (16.5)		10 (20.0)	10 (20.0)	0.00	
Gastric cancers	1 (1.3)	2 (1.7)		0 (0.0)	1 (2.0)	0.18	
Esophageal cancers	0 (0.0)	11 (9.6)		0 (0.0)	0 (0.0)	NA	
Hepatocellular carcinoma	3 (3.8)	2 (1.7)		1 (2.0)	2 (4.0)	0.10	
Oral carcinoma	2 (2.6)	3 (2.6)		0 (0.0)	1 (2.0)	0.13	
Biliary and pancreatic cancers	0 (0.0)	1 (0.9)		0 (0.0)	0 (0.0)	NA	
Other cancer types	6 (7.7)	6 (5.2)		3 (6.0)	4 (8.0)	0.07	
Lymphoma	8 (10.3)	6 (5.2)		5 (10.0)	5 (10.0)	0.00	
Mesothelioma	1 (1.3)	2 (1.7)		1 (2.0)	1 (2.0)	0.00	
Renal cell carcinoma	3 (3.8)	1 (0.9)		2 (4.0)	1 (2.0)	0.10	
Urogenital cancers	1 (1.3)	3 (2.6)		1 (2.0)	2 (4.0)	0.18	
Sarcoma	2 (2.6)	4 (3.5)		2 (4.0)	0 (0.0)	0.25	
Unknown types	10 (12.8)	17 (14.8)		8 (16.0)	6 (12.0)	0.12	
Whole-brain SUV$_{mean}$	4.61 (1.25)	4.63 (1.49)	0.92	4.72 (1.16)	4.54 (1.50)	0.15	0.45

*Independent t test (continuous) or χ^2 test (categoric).

†Wilcoxon signed-rank test (continuous), McNemar nonparametric test (binary), and χ^2 test (multiple categories).

SMD = standardized mean difference to show imbalance levels of variables after matching (variable with SMD > 0.25 is considered poorly matched); CHF = congestive heart failure; ECOG = Eastern Cooperative Oncology Group.

Data are number followed by percentage in parentheses, except for whole-brain SUV$_{mean}$, for which SD is given in parentheses.
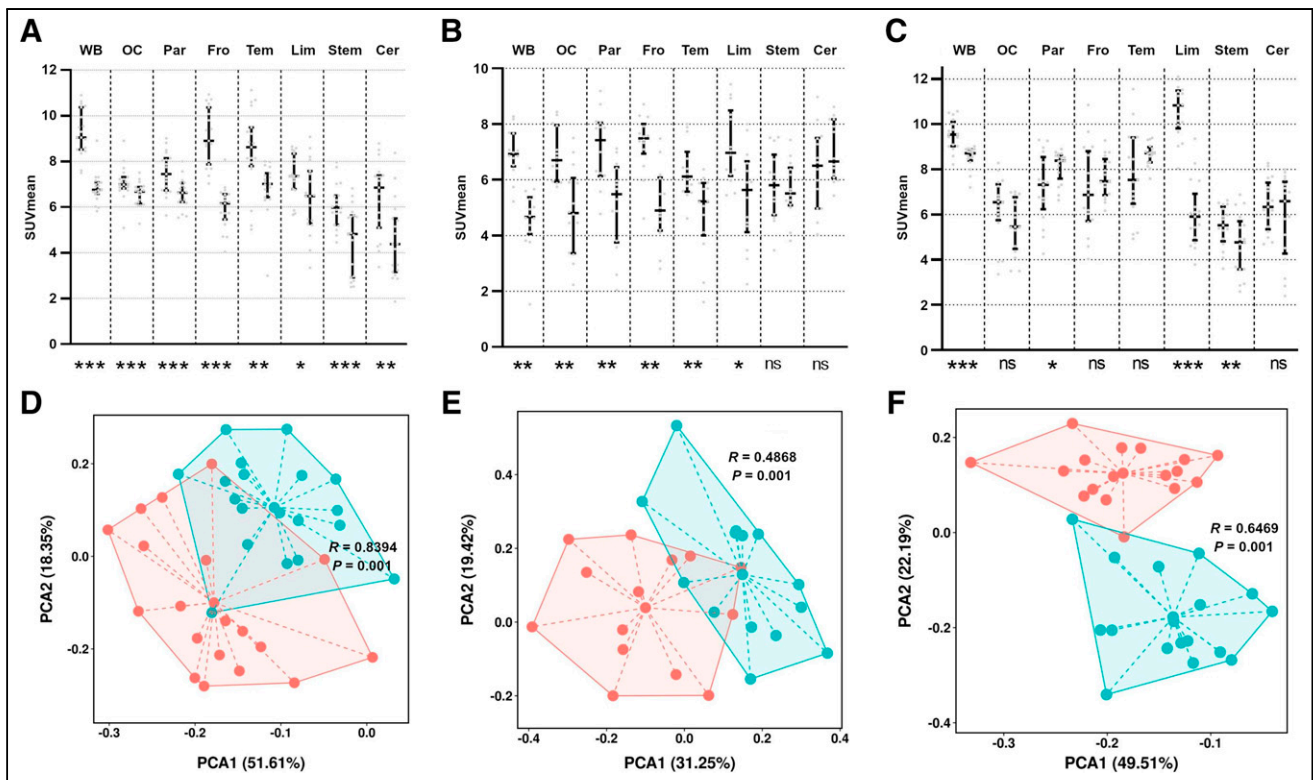
FIGURE 3. Comparison of regional uptake between CNSI and CNST subtypes. For each region, left side of plot is patients with infectious disease and right side is patients with immune-related disease. (A) SUV_{mean} distribution plot in infectious meningitis patients and immune-related meningitis patients in each brain lobe. Black lines indicate median and range (first to third quartiles). Wilcoxon signed rank was performed to compare distribution of SUV_{mean} between 2 subtypes. Significant difference in SUV_{mean} was seen in all regions of interest. (B) SUV_{mean} distribution plot in infectious meningoencephalitis patients and immune-related meningoencephalitis patients in each brain lobe. Black lines indicate median and range (first to third quartiles). Wilcoxon signed rank test was performed to compare distribution of SUV_{mean} between 2 subtypes. Significant difference in SUV_{mean} was seen in whole-brain area and in occipital, parietal, frontal, temporal, and limbic regions. (C) SUV_{mean} distribution plot in infectious encephalitis patients and immune-related encephalitis patients in each brain lobe. Black lines indicate median and range (first to third quartiles). Wilcoxon signed rank test was performed to compare distribution of SUV_{mean} between 2 subtypes. Significant difference in SUV_{mean} was seen in whole-brain area and in parietal, brain stein, and limbic regions. Intergroup difference was seen in meningitis diagnosis ($R = 0.84$) and in encephalitis ($R = 0.65$). (D–F) PCA of ^{18}F-FDG PET/CT radiomic uptake values to differentiate subtypes of meningitis (D), meningoencephalitis (E), and encephalitis (F). Intergroup difference in meningitis diagnosis ($R = 0.84$) and in encephalitis ($R = 0.65$). Cer = cerebellum; fro = frontal lobe; lim = limbic area; ns = nonsignificant; OC = occipital lobe; par = parietal lobe; PCA = principal-component analysis; stem = brain stem; tem = temporal lobe; WB = whole brain. *$P < 0.05$. **$P < 0.01$. ***$P < 0.001$.

Evaluating and Validating Preonset SUV_{mean} Changes as Marker to Predict Later CNST Incidence

We next investigated whether changes in brain regional metabolism were present before CNST onset. Sixty patients with available preonset ^{18}F-FDG PET/CT images were identified. The median time from ICI treatment to the earliest scanning was 12 wk (quartile range, 5.75–15.25 wk). The median time from the earliest scanning to CNST onset was 10 wk (quartile range, 8.75–14 wk).

Each regional SUV_{mean} was compared with the baseline value in CNST+ patients. There was a significant increase ($P < 0.01$) in SUV_{mean} as compared with baseline in all regions except the occipital lobe, brain stem, and cerebellum (Fig. 4A). The median SUV_{mean} increased from 4.83 to 4.88 in the whole brain, from 3.81 to 4.48 in the parietal lobe, from 4.30 to 4.44 in the frontal lobe, from 4.31 to 4.81 in the temporal lobe, from 3.84 to 4.52 in the limbic area, and from 4.92 to 5.04 in the cerebellum. These changes were validated in PSM samples (60 pairs) between CNST+ and CNST− patients. Changes in SUV_{mean} were significantly higher in CNST+ patients than in CNST− patients in the whole brain, frontal lobe, temporal lobe, and limbic area (Fig. 4B). The differentiating ability between CNST+ and CNST− patients

was evaluated using ROC curve analysis, with an AUC of 0.74 (Supplemental Fig. 6B), and a nomogram was drawn to quantify the risk of future CNST (Supplemental Fig. 6A).

In the independent validation cohort, we aimed to evaluate whether early regional changes in SUV_{mean} may predict the later incidence of CNST. We recruited 2,881 patients to undergo prognostic scanning and followed them up for 24 wk. Three patients were excluded because CNST occurred before prognostic scanning, and thus early changes of SUV_{mean} in ^{18}F-FDG PET/CT were evaluable in 2,878 patients (1,540 male and 1,338 female; mean age, 64.2 ± 5.79 y) for predictive ability. In total, 38 patients (24-wk incidence rate, 1.3%) were diagnosed with CNST, at a mean of 14.79 ± 6.66 wk after ICI initiation. A nomogram to quantify disease-free survival was thus drawn, with an AUC of 0.86 (95% CI, 0.79–0.94; Figs. 4C and 4D).

DISCUSSION

This pilot case-control study of multicenter samples investigated regional metabolism specific to CNST and evaluated the accuracy of preonset regional metabolic changes in predicting the future onset of CNST. CNST was also identified in ^{18}F-FDG PET/CT images as a
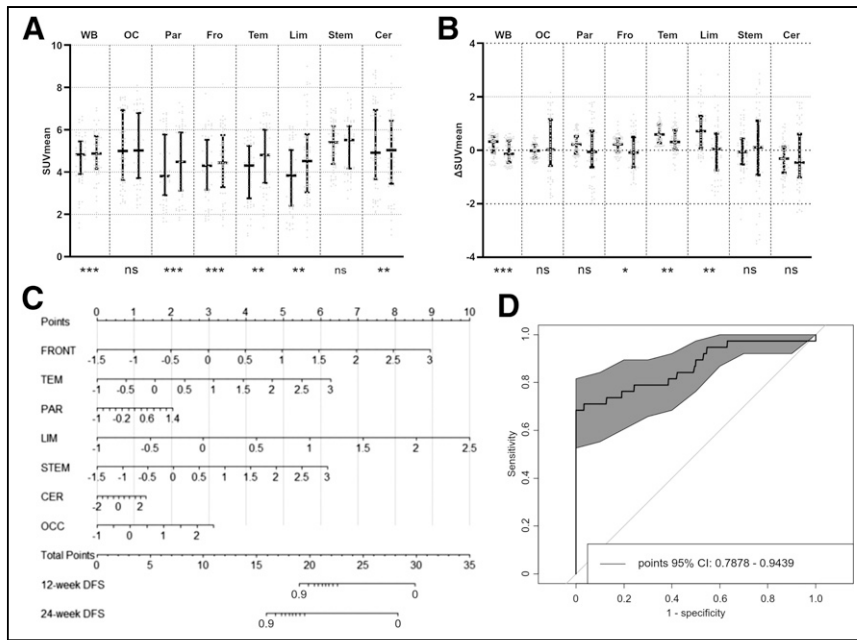
FIGURE 4. Comparison of regional uptake value changes before CNST onset. (A) Self-control comparison: SUV_{mean} distribution plot in CNST+ patients at baseline (before treatment, left side of plot for each region) and before CNST onset (right side of plot for each region) in each lobe. Black lines indicate median and range (first to third quartiles). SUV_{mean} in each region did not conform to normal distribution, and nonparametric Wilcoxon signed-rank test was performed to compare distribution at baseline and after CNST. Significant increases were seen in whole-brain area and in parietal, frontal, temporal, and limbic regions, and significant decreases were seen in cerebellum ($z = -3.50, -0.49, -3.51, -3.59, -6.73, -5.54, -0.45$, and -3.72, respectively, for rank differences in each comparison). (B) Negative control comparison: changes in SUV_{mean} from baseline to preonset scan in CNST+ patients (left side of plot for each region) and changes in SUV_{mean} from baseline to <5 mo after treatment in negative control (right side of plot for each region), matched by propensity scores. Black lines indicate median and range (first to third quartiles). Values did not conform to normal distribution, and nonparametric Wilcoxon signed-rank test was performed to compare distribution of changes in SUV_{mean} between 2 groups. Significant difference in changes in SUV_{mean} was seen in whole-brain area and in temporal, frontal, and limbic regions ($z = -3.69, -0.75, -1.39, -2.41, -6.61, -4.42, -0.25$, and -0.36, respectively, for rank differences in each comparison). (C) ^{18}F-FDG PET/CT radiomic monogram in validation cohort using early changes (5–6 wk after treatment initiation) of regional uptake values. Specifically, changes in SUV_{mean}, as compared with baseline SUV_{mean}, can be projected to point ruler. Total scores were added to obtain 24-wk disease-free survival probability. (D) Predicted future CNST risk vs. actual CNST risk in validation cohort, plotted as receiver-operating-characteristic curves. Cer = cerebellum; DFS = disease-free survival; fro and front = frontal lobe; lim = limbic area; ns = nonsignificant; OC and OCC = occipital lobe; par = parietal lobe; stem = brain stem; tem = temporal lobe; WB = whole brain. *$P < 0.05$. **$P < 0.01$. ***$P < 0.001$.

pathologic entity with specific regional hypermetabolism as compared with brain infection or CNST− patients. Prior case reports showed that the limbic area may be a prominent area of immune attack, and our results showed that hypermetabolism was seen in the whole brain and in the occipital, frontal, and temporal lobes. SUV_{mean} differed between CNST+ and CNSI in several regions—a positive control in terms of inflammation hypermetabolism (29). To our knowledge, our study was the first to analyze metabolism changes in brain immune-related adverse events after ICI treatment and the first to demonstrate that brain hypermetabolism, as a biomarker, may be present well before CNST symptoms exist. These regional metabolism differences were subsequently analyzed by radiomic methods, which showed moderate differentiating abilities. Early metabolism changes can be translated into a suggestive diagnostic tool. Considering the wide application of ^{18}F-FDG PET/CT in prognostic indexing of ICI-based treatment regimens, our pilot study may give initial evidence about quantitative biomarkers to assist CNST diagnosis. Given the extremely low incidence of CNST in ICI-treated cancer patients, with clinical characteristics similar to those of brain infection, use as a noninvasive,

quantitative tool to suggest levels of neuroinflammation during active ICI treatment may be a possibility.

Interestingly, early changes in cerebral metabolism were detected 10 wk (quartile range 8.75–14 wk) before CNST onset in a subgroup of patients ($n = 60$). Although the study recruited a relatively large sample size in terms of CNST incidence, subgroup statistical tests of differences in early changes as compared with CNST− patients may be underpowered to yield conclusive evidence and must be interpreted cautiously. However, the results may support an accumulative immune attack that may happen early before onset, as pointed out by radiologic evidence in other organs (14). Preclinical models also support autoimmunity before symptom onset (30). In our study, the earliest onset time for CNST+ patients with pre-onset ^{18}F-FDG PET/CT scans happened in the 12 wk after ICI treatment, suggesting a rather late onset. It should be noted that most cases of previously reported CNST had an early-onset symptom, usually beginning at the first month of ICI treatment. Thus, our preonset ^{18}F-FDG PET/CT scans may not be useful as a monitoring tool but rather suggest that immune attacks may occur even before clinical signs.

The ICIs used in our cohorts are all directed toward the programmed cell death protein 1 and programmed death ligand 1 pathways. However, currently, most immune-related reactions occur when ipilimumab, alone or in combination, is directed toward cytotoxic T-lymphocyte–associated protein 4. As such, what we report here may represent only one aspect, or a partial population, of CNST, and future research is encouraged to investigate immune-related adverse events inflicted by other types of immunotherapy (7–9). Also, ICIs may unmask, rather than induce, a preexisting inflammatory condition. As some patients may have an unreported history of mild autoimmune or rheumatic conditions, they may have an increased risk of CNST; this topic may require further investigation (31).

This study had some limitations. First, it had a retrospective design with uncontrolled recall bias in chart review. Second, the ^{18}F-FDG PET/CT scanning time, which was based on oncologist preference and tumor prognostic functions, could not be precisely matched between comparable groups. We chose ^{18}F-FDG PET/CT scanning after 5 mo of ICI therapy in CNST− patients to match the time period in CNST+ patients. Third, there are many confounders that can trigger regional metabolism changes. The SUV in our study was based on activity, weight, and injected dose, without further use of single-subject statistical parametric mapping analysis to normalize intensity. Lack of standardization in intensity normalization, with the correspondingly unknown effect on quantification output, may make the use of SUV in brain ^{18}F-FDG PET/CT quantification less accurate. The population was quite heterogeneous, as it

comprised patients with very different neoplasms in which ICI is often used in various combinations with chemotherapy—a potential cause of uncontrolled confounders during comparison (*10*). Also, age and sex were dictating factors in cerebral metabolism (*32*). Baseline factors were compared statistically, and several factors were significantly different as shown in Table 1. However, the PSM method, which included multiple baseline confounders in this study, partially salvaged the selection bias. Last, although the sample size was relatively large in the context of the extreme low incidence of CNST, statistical power remained low in matched comparisons, especially in the comparison statistics of matched subtypes of CNST versus CNSI. Future metaanalyses or large-sample research is encouraged to augment the statistical power.

CONCLUSION

Cerebral metabolism seemed increased in CNST+ patients on active ICI therapy as compared with CNST− patients but seemed lower than in CNSI patients in certain brain regions. Early regional changes that were present before CNST seemed to suggest a preonset immune attack, and such early regional changes may be translated into a diagnostic tool based on moderate accuracy in the observational study.

DISCLOSURE

ACKNOWLEDGMENT

KEY POINTS

QUESTION: What are the probable biomarkers specific to immune-related CNST in cancer patients treated with ICI by imaging analysis of ^{18}F-FDG PET/CT?

PERTINENT FINDINGS: In a validation cohort of 2,878 patients, preonset changes in SUV$_{mean}$ reached an AUC of 0.86 (95% CI, 0.79–0.94) in predicting the later incidence of CNST.

IMPLICATIONS FOR PATIENT CARE: Regional SUV differences may be translated into early diagnostic tools based on moderate differentiating accuracy in our study.

REFERENCES

1. Kruger S, Ilmer M, Kobold S, et al. Advances in cancer immunotherapy 2019: latest trends. *J Exp Clin Cancer Res.* 2019;38:268.
2. Horvat T, Adel N, Dang T, et al. Immune-related adverse events, need for systemic immunosuppression, and effects on survival and time to treatment failure in patients with melanoma treated with ipilimumab at Memorial Sloan Kettering Cancer Center. *J Clin Oncol.* 2015;33:3193–3198.
3. Postow MA, Sidlow R, Hellmann M. Immune-related adverse events associated with immune checkpoint blockade. *N Engl J Med.* 2018;378:158–168.
4. Jing Y, Liu J, Ye Y, et al. Multi-omics prediction of immune-related adverse events during checkpoint immunotherapy. *Nat Commun.* 2020;11:4946.
5. Wick W, Hertenstein A, Platten M. Neurological sequelae of cancer immunotherapies and targeted therapies. *Lancet Oncol.* 2016;17:e529–e541.
6. Perrinjaquet C, Desbaillets N, Hottinger AF. Neurotoxicity associated with cancer immunotherapy: immune checkpoint inhibitors and chimeric antigen receptor T-cell therapy. *Curr Opin Neurol.* 2019;32:500–510.
7. Johnson DB, Manouchehri A, Haugh AM, et al. Neurologic toxicity associated with immune checkpoint inhibitors: a pharmacovigilance study. *J Immunother Cancer.* 2019;7:134.
8. Guidon AC, Burton LB, Chwalisz BK, et al. Consensus disease definitions for neurologic immune-related adverse events of immune checkpoint inhibitors. *J Immunother Cancer.* 2021;9:e002890.
9. Winter SF, Vaios EJ, Dietrich J. Central nervous system injury from novel cancer immunotherapies. *Curr Opin Neurol.* 2020;33:723–735.
10. Vogrig A, Muñiz-Castrillo S, Farina A, Honnorat J, Joubert B. How to diagnose and manage neurological toxicities of immune checkpoint inhibitors: an update. *J Neurol.* 2022;269:1701–1714.
11. Spain L, Diem S, Larkin J. Management of toxicities of immune checkpoint inhibitors. *Cancer Treat Rev.* 2016;44:51–60.
12. Larson SM. Cancer or inflammation? A holy grail for nuclear medicine. *J Nucl Med.* 1994;35:1653–1655.
13. Dimitrakopoulou-Strauss A. Monitoring of patients with metastatic melanoma treated with immune checkpoint inhibitors using PET-CT. *Cancer Immunol Immunother.* 2019;68:813–822.
14. Hribernik N, Huff DT, Studen A, et al. Quantitative imaging biomarkers of immune-related adverse events in immune-checkpoint blockade-treated metastatic melanoma patients: a pilot study. *Eur J Nucl Med Mol Imaging.* 2022;49:1857–1869.
15. Bordonne M, Chawki MB, Doyen M, et al. Brain ^{18}F-FDG PET for the diagnosis of autoimmune encephalitis: a systematic review and a meta-analysis. *Eur J Nucl Med Mol Imaging.* 2021;48:3847–3858.
16. Solnes LB, Jones KM, Rowe SP, et al. Diagnostic value of ^{18}F-FDG PET/CT versus MRI in the setting of antibody-specific autoimmune encephalitis. *J Nucl Med.* 2017;58:1307–1313.
17. Rissanen E, Carter K, Cicero S, et al. Cortical and subcortical dysmetabolism are dynamic markers of clinical disability and course in anti-LGI1 encephalitis. *Neurol Neuroimmunol Neuroinflamm.* 2022;9:e1136.
18. Yshii LM, Hohlfeld R, Liblau RS. Inflammatory CNS disease caused by immune checkpoint inhibitors: status and perspectives. *Nat Rev Neurol.* 2017;13:755–763.
19. Joly F, Castel H, Tron L, Lange M, Vardy J. Potential effect of immunotherapy agents on cognitive function in cancer patients. *J Natl Cancer Inst.* 2020;112:123–127.
20. Chow SC, Shao J, Wang H, Lokhnygina Y. *Sample Size Calculations in Clinical Research.* Chapman and Hall/CRC; 2017:373–383.
21. Tzourio-Mazoyer N, Landeau B, Papathanassiou D, et al. Automated anatomical labeling of activations in SPM using a macroscopic anatomical parcellation of the MNI MRI single-subject brain. *Neuroimage.* 2002;15:273–289.
22. Clarke KR. Non-parametric multivariate analyses of changes in community structure. *Austral Ecol.* 1993;18:117–143.
23. Warton DI, Wright ST, Wang Y. Distance-based multivariate analyses confound location and dispersion effects. *Methods Ecol Evol.* 2012;3:89–101.
24. Yun M, Nie B, Wen W, et al. Assessment of cerebral glucose metabolism in patients with heart failure by ^{18}F-FDG PET/CT imaging. *J Nucl Cardiol.* 2022;29:476–488.
25. Lyra V, Parissis J, Kallergi M, et al. ^{18}F-FDG PET/CT brain glucose metabolism as a marker of different types of depression comorbidity in chronic heart failure patients with impaired systolic function. *Eur J Heart Fail.* 2020;22:2138–2146.
26. Johnson NA, Jahng GH, Weiner MW, et al. Pattern of cerebral hypoperfusion in Alzheimer disease and mild cognitive impairment measured with arterial spin-labeling MR imaging: initial experience. *Radiology.* 2005;234:851–859.
27. Fleiss JL, Levin B, Paik MO. *Statistical Methods for Rates and Proportions.* 3rd ed. John Wiley & Sons, Inc. 2003:373–406.
28. Austin PC. Balance diagnostics for comparing the distribution of baseline covariates between treatment groups in propensity-score matched samples. *Stat Med.* 2009;28:3083–3107.
29. Müller-Jensen L, Zierold S, Versluis JM, et al. Characteristics of immune checkpoint inhibitor-induced encephalitis and comparison with HSV-1 and anti-LGI1 encephalitis: a retrospective multicentre cohort study. *Eur J Cancer.* 2022;175:224–235.
30. Iwama S, De Remigis A, Callahan MK, Slovin SF, Wolchok JD, Caturegli P. Pituitary expression of CTLA-4 mediates hypophysitis secondary to administration of CTLA-4 blocking antibody. *Sci Transl Med.* 2014;6:230ra45.
31. Lusa A, Alvarez C, Saxena Beem S, Schwartz TA, Ishizawar R. Immune-related adverse events in patients with pre-existing autoimmune rheumatologic disease on immune checkpoint inhibitor therapy. *BMC Rheumatol.* 2022;6:64.
32. Jones JS, Goldstein SJ, Wang J, et al. Evaluation of brain structure and metabolism in currently depressed adults with a history of childhood trauma. *Transl Psychiatry.* 2022;12:392.